Computer Networks 53 (2009) 2458–2475

Contents lists available at ScienceDirect

Computer Networks

journal homepage: www.elsevier.com/locate/comnet

Two and three-dimensional intrusion object detection under randomized scheduling algorithms in sensor networks

Yang Xiao [a,*], Yanping Zhang [a], Miao Peng [a], Hui Chen [b], Xiaojiang Du [c], Bo Sun [d], Kui Wu [e]

[a] Dept. of Computer Science, Univ. of Alabama, United States
[b] Dept. of Mathematics and Computer Science, Virginia State Univ., United States
[c] Dept. of Computer and Information Sciences, Temple Univ., United States
[d] Dept. of Computer Science, Lamar Univ., United States
[e] Dept. of Computer Science, Univ. of Victoria, Canada

ARTICLE INFO

Article history:
Received 18 June 2008
Received in revised form 30 April 2009
Accepted 3 May 2009
Available online 19 May 2009

Responsible Editor: J. Lopez

Keywords:
Wireless sensor network
Randomized scheduling algorithm
Coverage
Intrusion object
Energy consumption
Two-dimensional
Three-dimensional

ABSTRACT

We are interested in wireless sensor networks which are used to detect intrusion objects such as enemy tanks, cars, submarines, etc. Since sensor nodes have a limited energy supply, sensor networks are configured to put some sensor nodes in sleep mode to save energy. This is a special case of a randomized scheduling algorithm. Ignored by many studies, an intrusion object's size and shape are important factors that greatly affect the performance of sensor networks. For example, an extremely large object in a small sensor field can easily be detected by even one sensor node, no matter where the sensor node is deployed. The larger an intrusion object is, the fewer sensor nodes that are required for detection. Furthermore, using fewer sensor nodes can save resources and reduce the waste of dead sensor nodes in the environment. Therefore, studying coverage based on intrusion object's size is important. In this paper, we study the performance of the randomized scheduling algorithm via both analysis and simulation in terms of intrusion coverage intensity. In particular, we study cases where intrusion objects occupy areas in a two-dimensional plane and where intrusion objects occupy areas in a three-dimensional space, respectively. We also study the deployment of sensor nodes when intrusion objects are of different sizes and shapes. First, sensor nodes are deployed in a two-dimensional plane and a three-dimensional space with uniform distributions. Then, they are deployed in a two-dimensional plane and a three-dimensional space in two-dimensional and three-dimensional Gaussian distributions, respectively. Therefore, our study not only demonstrates the impact of the size and shape of intrusion objects on the performance of sensor networks, but also provides a guideline on how to configure sensor networks to meet a certain detecting capability in more realistic situations.

1. Introduction

Wireless sensor networks (WSNs) have become an important technology, combining sensing technology, embedded computing, distributed information processing, and wireless communication technology [25,26,38–74]. WSNs have broad applications [6,27], such as medical monitoring, environment pollution monitoring, forest fire monitoring, target tracking, combat field reconnaissance, and military command and control, and so on. Data collection is the basic objective of in these applications. Data collection capability of a sensor network depends on its sensing coverage and network connectivity. Sensor nodes are often powered by batteries, and it is often difficult or

* Corresponding author. Tel.: +1 205 348 4038.
E-mail addresses: yangxiao@ieee.org (Y. Xiao), yzhang@cs.ua.edu (Y. Zhang), mpeng@ua.edu (M. Peng), huichen@ieee.org (H. Chen), dxj@ieee.org (X. Du), bsun@my.lamar.edu (B. Sun), wkui@ieee.org (K. Wu).

1389-1286/$ - see front matter © 2009 Elsevier B.V. All rights reserved.
doi:10.1016/j.comnet.2009.05.002

impossible to recharge the deployed nodes. Great efforts [1,2,7,8,10–12] have been devoted to minimizing the energy consumption and extending the lifetime of the network.

Although energy efficiency is the essential requirement for WSNs, it should not be achieved at the cost of reducing network coverage, which is usually a major Quality of Service (QoS) metric of WSNs [23]. As sensor nodes are usually densely deployed, they are often highly spatially-redundant [20]. Therefore, energy efficiency and high sensing coverage can be achieved simultaneously by exploiting the spatial redundancy among sensor nodes. Many research efforts have been devoted to sensor scheduling algorithms that turn off redundant sensor nodes for energy saving [1–5,7,14,17].

Since maintaining location information and time synchronization introduces extra energy and computational overhead, some scheduling schemes [1,7,9,13,19] do not require location information or precise time synchronization of sensor nodes. In [16], the authors proposed several sensing scheduling protocols and analyze the performance of object detection and network lifetime. The joint problem of coverage and connectivity were considered recently in [9,15,18,22]. In [18], the authors considered a network with sensor nodes deployed strictly in grids. The joint problem in more general sensor networks where the sensor nodes are deployed at random was investigated in [9,22]. Similar work was done in [21], in which the authors also present a Coverage Configuration Protocol (CCP) that can provide fully coverage of a convex region. In [9–11,24], the authors have studied a k-set randomized scheduling algorithm where sensor nodes are randomly divided into k disjoint subsets (S_j; $j = 1,2,\ldots,k$) that work alternatively. In other words, at any time, only one set of sensor nodes are working, and the rest of the sensor nodes sleep.

Many studies only consider cases where intrusion objects are modeled as a point on a two-dimensional plane. In reality, an intrusion object is far larger than a point. In a sensor network deployed to detect enemy tanks or to detect people crossing a country's boundary, intrusion objects' sizes are totally different. A tank's size could be larger than the sum of the sensing range of several sensor nodes. We observed that the larger an intrusion object, the more likely it is that the intrusion object will be detected, and the fewer sensor nodes are required.

Furthermore, sensor nodes and intrusion objects are not necessarily on a two-dimensional plane, and the shapes of the intrusion objects often span intro three-dimensional space. For example, in an underwater sensor network, sensor nodes may be deployed in different depths to detect enemy submarines or other underwater intrusion robots. Another example is warehouse monitoring, in which sensor nodes are deployed on shelves to monitor goods in a warehouse. The sensing area is in fact three-dimensional, and the monitored area and objects always occupy a three-dimensional space. The size and shape of an intrusion object have impacts on the sensing capability of sensor networks. Therefore, in many applications, three-dimensional considerations are more realistic. Meanwhile, the sensing area of a sensor node should be also considered to be a three-dimensional space.

In this paper, we first study the intrusion coverage intensity via both analysis and simulation when the intrusion object occupies an area in a two-dimensional plane. The intrusion coverage intensity is defined as the probability that a given area at a given time is detected by at least one active sensor node. Furthermore, we study the intrusion coverage intensity of intrusion objects occupying a three-dimensional space, and the sensing fields of sensor nodes are expressed as spheres. To further approach reality, we study the case when sensor nodes are deployed using non-uniform distributions. In these scenarios, we study how the sizes and shapes of the intrusion objects influence the sensor network's configuration. Thus, through the study, we provide a guideline on the number of sensor nodes needed to meet certain levels of intrusion coverage intensity in more realistic settings.

The rest of the paper is organized as follows. We introduce related work on object detection in sensor networks in Section 2. In Section 3, we analyze the intrusion coverage intensity of K-set randomized scheduling algorithms when intrusion objects are abstracted to 2D and 3D shapes, respectively. In Sections 4 and 5, the results are extended to more realistic cases, in which sensor node deployment follows Gaussian distribution in a two-dimensional plane and a three-dimensional space, respectively. In Section 6, we focus on answering a few practical questions, such as how the size and shape of intrusion objects affect the detecting capability of sensor networks via performance evaluation using both analysis and computer simulations. Finally, we conclude our paper in Section 7.

2. Related work

Many efforts in WSNs have been dedicated to tracking and locating objects. In [32], a technique that employs the false discovery rate (FDR) procedure and belief propagation (BP) like algorithm is proposed for detection and localization problems in sensor networks. In [35], cooperative tracking, which combines acoustic information detected from neighboring sensor nodes and estimates the location of objects, was proposed as a method for tracking objects. In [28], the authors provided an upper limit to how far a mobile intrusion object can reach along a straight line within a dense wireless sensor network before it is detected.

According to the features of wireless sensor networks, energy consumption is an invariable problem in any application of wireless sensor networks. In [33], a semantic location-based data model for object tracking sensor networks was proposed in order to achieve network-wide energy optimization. The strategy directs data dissemination of and data extraction from sensor nodes in a power-efficient way. Meanwhile, to save energy, many researchers develop strategies that periodically switch off sensor nodes. In [29,31], the trade-offs between the speed of detecting the mobile object and the energy savings brought by turning many nodes into sleep mode were examined. In [29], the authors quantified the trade-off between power conservation and the quality of object tracking while presenting guidelines for efficient deployment of

sensor nodes for target tracking applications. *K*-set randomized scheduling algorithm [9–11,24] is an algorithm that divides all sensor nodes into *k* disjoint sets, in which only one set of sensor nodes is working at any time while the rest of the sensor nodes are sleeping.

In [34], multiple-object detection is discussed, and based on a Gaussian mixture model [36] and Expectation/Maximization (EM) clustering [37], techniques for boosting detector accuracy by fitting a world model to detections from multiple locations are explored. A modified EM clustering algorithm is employed to solve the data association problem for an arbitrary number of views, and a fast maximum-likelihood solution is found without resorting to an explicit correspondence search.

Most studies do not consider the size and the shape of the intrusion object. However, every intrusion object has a size and a shape which greatly impact the detection and the deployment of sensor nodes as well. An extreme example is that when the intrusion object is as large as the size of the sensing field, one sensor node is enough for detecting the presence of the object, no matter how small its sensing range is. Furthermore, the larger an intrusion object is, the more likely it is that it will be detected. In other words, with the same likelihood being detected, we need fewer sensor nodes. Using fewer sensor nodes can also save resources and reduce the waste of dead sensor nodes in the environment. In a different application, intrusion objects such as armored vehicles and land mines, are also different in shape. In this scenario, sensor nodes could be more efficiently deployed according to sizes and shapes of different intrusion objects. Furthermore, in some applications, it would be unrealistic to assume that all objects and sensor nodes appear in a two-dimensional plane. For example, in an underwater sensor network used to detect enemy submarines, sensor nodes and enemy submarines may appear in different depths. Another example would be a sensor network used to detect merchandise, vehicles, and workers in a warehouse where objects can appear in different sizes and shares with sensor nodes deployed on the roof, the floor, and the shelves. The sizes, shapes, and positions of objects certainly affect the sensing capability of sensor networks. Thus, it will help understand the performance and deployment of sensor networks by studying sensor network scheduling algorithms, not only in a two-dimensional plane, but also in a three-dimensional space, which is the main focus of this work.

3. 2D and 3D intrusion object

Previous work in [5,9–11,24,75] assumes that an intrusion object is one point in the sensor field. In this paper, we assume that the intrusion object occupies an area (2D) or space (3D), which will be denoted by *o*. Of course, the intrusion object's size is difficult to predict beforehand. However, studying it can help to set up a sensor network's configuration. For example, in a sensor network deployed to detect enemy tanks or people crossing a country's boundary, intrusion objects' sizes are totally different. Larger size would correspond to larger detection probability, that is, ease of detection. Therefore, fewer sensor nodes are required for the detection of a larger object. This section studies the influence of the sizes of intrusion objects on a sensor network's configuration, e.g., the influence of the number of deployed sensor nodes. Intuitively, the smaller the intrusion objects, the more sensor nodes deployed. Meanwhile, the intrusion objects are modeled with two different considerations: two-dimensional (2D) and three-dimensional (3D) cases.

3.1. Per-sensor detection probability of 2D situation

Assume that all sensor nodes are developed in a two-dimensional plane. In many applications, when an object is an armored vehicle such as a tank, we can abstract it as a rectangle; and when an object is a land mine, we can abstract it as a circle. Rectangles and circles are first-order approximations of many different shapes. Thus, we choose rectangle and circle as the shapes of intrusion objects in the 2D situation.

We first derive the probability, denoted as p_1, that a sensor node can detect an intrusion object with size *o* in the 2D situation. It is equal to the probability that a random sensor node's area overlaps the area of a random intrusion object. In order to derive the probability, we assume that the object shape is either a rectangle (with its length b and width o/b) or a circle (with $2\sqrt{o/\pi}$ as the diameter). We also assume that a sensor node's coverage area is a circle. We use Φ to denote the sensing area of a sensor node.

As illustrated in Fig. 1, a sensor node does not overlap an intrusion object if the sensor node's center is far away ($> \sqrt{\Phi/\pi}$) from the boundary of the intrusion object. The probability that a sensor node detects an intrusion object with a circular or rectangular shape is expressed as follows:

$$\begin{aligned} p_1 &= \Pr(\text{a sensor detects an intrusion object}) \\ &= \Pr(\text{a sensor area overlaps the area of object}) \\ &= \begin{cases} \frac{\pi}{a}\left(\sqrt{\Phi/\pi}+\sqrt{o/\pi}\right)^2, & \text{circle} \\ \frac{1}{a}\left(o+2(b+o/b)\sqrt{\Phi/\pi}+\Phi\right), & \text{rectangle} \end{cases} \\ &= \begin{cases} \frac{1}{a}\left(\sqrt{\Phi}+\sqrt{o}\right)^2, & \text{circle}, \\ \frac{1}{a}\left(o+2(b+o/b)\Phi\sqrt{r/\pi}+\Phi\right), & \text{rectangle}. \end{cases} \end{aligned} \tag{1}$$

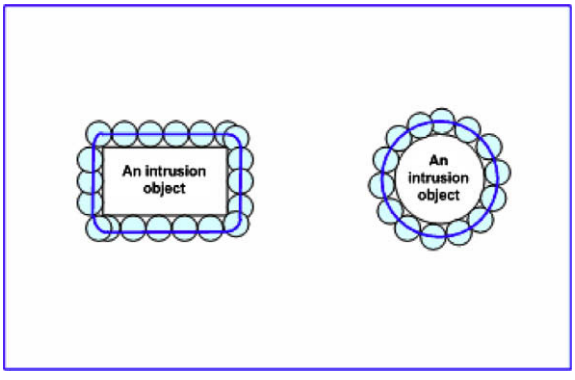

Fig. 1. Sensor node's range overlaps an intrusion object.

3.2. Per-sensor detection probability of 3D situation

The sensing range of real-world sensor devices is subject to the orientation and aperture of the sensor nodes. Furthermore, a sensor node can physically carry several sensors, with each monitoring a different direction. For ease of analysis, we assume that a sensor node can monitor the activities within a spherical space in the 3D situation. We consider objects of two different shapes, spherical and cuboid, which are first-order approximations of many detectable objects such as submarines, surface warships, and water mines.

We assume that the sensing area of a sensor node is also a ball, and that the sensing radius of a sensor node is $\sqrt[3]{3\Phi/(4\pi)}$. Let o denote the size of an intrusion object, which is the space which the object occupies. If the object is spherical, its radius is $\sqrt[3]{3o/(4\pi)}$. If the object is cuboid, we denote its length, width, and height as b, c, and $o/(bc)$, respectively. A sensor node does not overlap an intrusion object if the sensor node is far away ($> \sqrt[3]{3\Phi/(4\pi)}$) from the boundary of the intrusion object. The probability that a sensor node detects a spherical or cuboid intrusion object is expressed as follows, as well as shown in Fig. 2:

$$\begin{aligned} p_1 &= \Pr(\text{a sensor detects an intrusion object}) \\ &= \Pr(\text{a sensor area overlaps the body of object}) \\ &= \begin{cases} \frac{4\pi}{3a}\left(\sqrt[3]{3\Phi/(4\pi)} + \sqrt[3]{3o/(4\pi)}\right)^3, & \text{spherical} \\ \frac{1}{a}[o + 2(bc + o/b + o/c)\sqrt[3]{3\Phi/(4\pi)} \\ \quad +\Phi + (b + c + o/(bc))\pi\left(\sqrt[3]{3\Phi/(4\pi)}\right)^2], & \text{cuboid} \end{cases} \\ &= \begin{cases} \frac{1}{a}\left(\sqrt[3]{\Phi} + \sqrt[3]{o}\right)^3, & \text{spherical}, \\ \frac{1}{a}[o + 2(bc + o/b + o/c)\sqrt[3]{3\Phi/(4\pi)} \\ \quad +\Phi + (b + c + o/(bc))\sqrt[3]{9\pi\Phi^2/16}], & \text{cuboid}. \end{cases} \end{aligned} \tag{2}$$

3.3. Intrusion detection/coverage intensity

First of all, we should re-consider the definition of network coverage intensity [9–11,24,75] expressed in (3), which may not be proper for large intrusion objects in a 2D or 3D situation

$$C_n = 1 - [1 - \Phi/(ak)]^n. \tag{3}$$

In (3), Φ, a, and k denote the size of the sensing area of each sensor node, the size of the whole sensing field, and the number of disjointed subsets, respectively. Therefore, Φ/a is the probability that a sensor node covers a given point.

Let p_1 be the probability that an object is within the sensing range of a sensor node. For our study of intrusion detection, we define intrusion detection/coverage intensity V_n as follows:

$$V_n = 1 - [1 - p_1/k]^n. \tag{4}$$

From (4), we know that the intrusion detection intensity is the probability that a given area at a given time is detected by at least one active sensor node.

3.4. Sensor network deployment

We now study the number of sensor nodes or the number of subsets required to achieve a certain degree of intrusion detection intensity when the intrusion object occupies an area or space. For example, in a sensor network deployed to detect enemy tanks or people crossing a country's boundary, intrusion objects' sizes are totally different. Meanwhile, the monitored area may be airspace or water area, and the object may be an airplane or submarine. Sensor nodes are randomly deployed in the monitored area. They might be some smart dust [30] that floats in the air or they might be some underwater sensor nodes. The following two questions need to be answered in order to investigate the influence of the sizes of intrusion objects on a sensor network's configuration, e.g., the number of sensor nodes that are needed to be deployed.

- Question A: given intrusion coverage/detection intensity and the size of the intrusion object [(o,b) of 2D object and (o,b,c) of 3D object], what is the minimum number of sensor nodes needed to achieve the intrusion detection intensity requirement?
- Question B: given intrusion coverage/detection intensity and the size of the intrusion object [(o,b) of 2D object and (o,b,c) of 3D object], what is the maximum k value that will achieve the intrusion detection intensity requirement?

From (3) and (4), we have the following results:

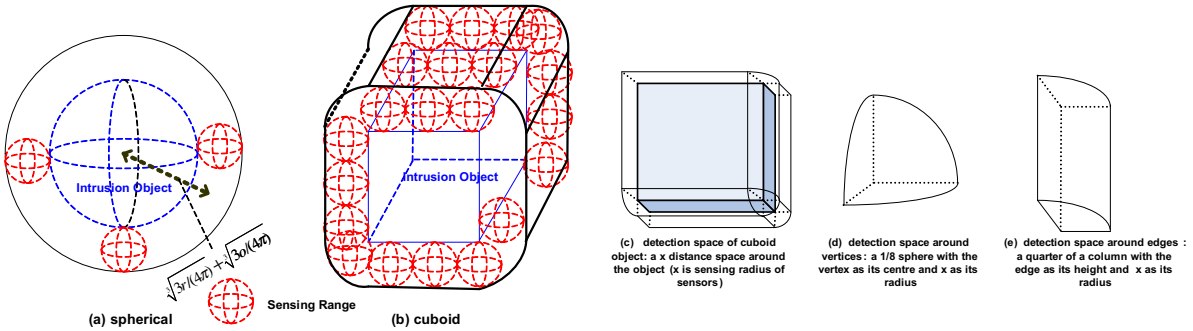

Fig. 2. 3D intrusion objects.

Lemma 1. *Given a required intrusion coverage/detection intensity $V_{n\text{-}req}$, the minimum number of sensor nodes to achieve $V_{n\text{-}req}$ is at least*

$$n \geqslant \frac{\ln(1 - V_{n\text{-}req})}{\ln(1 - p_1/k)}. \tag{5}$$

The above result answers Question A.

Lemma 2. *Given a required intrusion coverage/detection intensity $V_{n\text{-}req}$, the maximum number of subsets to achieve $V_{n\text{-}req}$ is*

$$k \leqslant \frac{p_1}{\left(1 - (1 - V_{n\text{-}req})^{1/n}\right)}. \tag{6}$$

The above result answers Question B.

3.5. Asymptotic detection and other properties

In this subsection, we derive and study asymptotic coverage, as well as other properties. From (2), we can easily get the following lemma:

Lemma 3. *Intrusion coverage/detection intensity is an increasing function of n and $\lim_{n\to\infty} V_n = 1$ holds. Intrusion coverage/detection intensity is a decreasing function of k, and $\lim_{k\to\infty} V_n = 0$ holds.*

Lemma 1 implies that, given a fixed number of subsets (k), any intrusion detection intensity can be achieved by increasing the number of sensor nodes deployed, and that given a fixed number of sensor nodes deployed, increasing the number of subsets (k) decreases intrusion detection intensity. These are consistent with our intuition.

Assuming that k and n are proportional such that $n = km$, where m is the number of sensor nodes per subset/shift, we have

$$\lim_{\substack{k=n/m \\ n\to\infty}} V_n = 1 - \lim_{n\to\infty}\left(1 - \frac{p_1 m}{n}\right)^n = 1 - e^{-p_1 m} \triangleq V(m), \tag{7}$$

where $V(m)$ is a function of the number of sensor nodes per shift (m). V_n is an interesting feature of intrusion coverage/detection intensity. We have

Lemma 4. (1) $V(m) \triangleq \lim_{k=n/m} V_n = 1 - e^{-p_1 m}$; (2) $\lim_{m\to\infty} V(m) = 1$; (3) $\lim_{p_1\to\infty} V(m) \overset{n\to\infty}{=} 1$.

3.6. Sensor deployment optimization

Lemma 5. *For a 2D intrusion object with a rectangular shape, the minimal intrusion coverage intensity $\min(V_n)$ is achieved when $b = \sqrt{o}$, where*

$$\min(V_n) = 1 - \left[1 - \left(\frac{1}{a}\left(o + 4\sqrt{o\Phi/\pi} + \Phi\right)\right)\Big/ k\right]^n. \tag{8}$$

Proof. Obtaining the minimal $V_n = 1 - [1 - p_1/k]^n$ is equivalent to obtaining the minimal p_1. From (1), we have, $p_1 = \frac{1}{a}\left(o + 2(b + o/b)\sqrt{r/\pi} + r\right)$, and obtaining the minimal p_1 is equivalent to obtaining the minimal $b + o/b$.

Let $f(b) = b + \frac{o}{b}, b > 0, o > 0$. We derive $f'(b)$ as follows: $f'(b) = 1 - \frac{o}{b^2}$. Because $b > 0$, $o > 0$, when $f'(b) = 0$ we have $b = \sqrt{o}$. Furthermore, we know if $b < \sqrt{o}$, we have $f'(b) < 0$, i.e., $f(x)$ is an decreasing function. On the other hand, if $b > \sqrt{o}$, we have $f'(b) > 0$, i.e., $f(b)$ is an increasing function. Therefore, when $b = \sqrt{o}, f(b)$ achieves the minimum. Therefore, $\min(b + o/b)$ is achieved when $b = \sqrt{o}$.

Therefore, by plugging $b = \sqrt{o}$ back to (1) and (4), we obtain (8). □

Lemma 6. *For a 3D intrusion object with a cuboid shape, the minimal intrusion detection intensity $\min(V_n)$ is achieved when $b = c = \sqrt[3]{o}$, where*

$$\min(V_n) = 1 - \left\{1 - \frac{1}{ak}\left(o + 6\sqrt[3]{3\Phi o^2/(4\pi)} + \Phi + 3\sqrt[3]{9\pi\Phi^2 o/16}\right)\right\}^n. \tag{9}$$

Proof. First, when $b = c = \sqrt[3]{o}$, we have $p_1 = \frac{1}{a}(o + 6\sqrt[3]{3\Phi o^2/(4\pi)} + \Phi + 3\sqrt[3]{9\pi\Phi^2 o/16})$ and $V_n = 1 - [1 - p_1/k]^n = 1 - \left\{1 - \frac{1}{ak}\left(o + 6\sqrt[3]{3\Phi o^2/(4\pi)} + \Phi + 3\sqrt[3]{9\pi\Phi^2 o/16}\right)\right\}^n$. Therefore, the only thing to prove is that $b = c = \sqrt[3]{o}$ achieves the minimum. Obtaining the minimal $V_n = 1 - [1 - p_1/k]^n$ is equivalent to obtaining the minimal p_1. From (2), we have $p_1 = \frac{1}{a}\left[o + 2(bc + o/b + o/c)\sqrt[3]{3\Phi/(4\pi)} + \Phi + (b + c + o/(bc))\sqrt[3]{9\pi\Phi^2/16}\right]$, and obtaining the minimal p_1 is equivalent to obtaining the minimal for both $f = bc + o/b + o/c$ and $g = b + c + o/(bc)$ with the same parameters.

For $b > 0$, $c > 0$, $o > 0$, we have $bc > 0, o/b > 0$, $o/c > o$, then $bc + o/b + o/c \geqslant 3\sqrt[3]{(bc)(o/b)(o/c)} = 3\sqrt[3]{o^2}$ ("=" holds when $bc = o/b = o/c$). That is, $f = bc + o/b + o/c \geqslant 3\sqrt[3]{o^2}$ ("=" holds when $b = c = \sqrt[3]{o}$). Similarly, we can prove that $g = b + c + o/(bc) \geqslant 3\sqrt[3]{bco/(bc)} = 3\sqrt[3]{o}$ ("=" when $b = c = \sqrt[3]{o}$). Therefore, $b = c = \sqrt[3]{o}$ achieves the minimal value for p_1. □

3.7. Projection approach

One intuition is to solve the 3D case by projecting a 3D intrusion object and sensing range into 2D planes (i.e., xy, xz, yz) under the assumption that both the intrusion object and the sensing range are convex, and two convex objects intersect in the 3D if and only if the projections of the objects intersect on all three 2D planes.

However, the above intuition is not correct. For a spherical object, its projections are three circle areas with sizes equal to $\pi\left[\sqrt[3]{3\Phi/(4\pi)}\right]^2$. However, considering an object which has projections of the exact three circle areas with sizes equal to $\pi\left[\sqrt[3]{3\Phi/(4\pi)}\right]^2$, the object may be larger than the spherical object.

In Fig. 3, a three-dimensional object (Q) is made by three orthogonal cylinders. Its projections on these 2D planes (xy, yz, zx) are exactly the same as the projections of a sphere, which are three circular areas with the same

size. The assumption is that the radius of the cylinder is equal to the radius of the sphere, and that Q and the sphere share the same center. The sphere is inside the object Q.

However, Q is totally different from the sphere. They only share at most three tangent circle lines on their surface. That is because, each cylinder only shares a circle line with the sphere on the surface, which is the tangency. Then the three cylinders and the sphere totally share three circle lines on their surfaces. The surfaces of Q are formed by these three cylinders. In other words, all the points on the surface of Q are on the surface of these three cylinders. Therefore, the common points between Q and the sphere are at most these three circle lines. In fact, Q and the sphere share these three circle lines on their surface.

Therefore, we can achieve a three-dimensional object Q, that has the same projections as a sphere, but only shares three circle lines on its surface. Therefore, they have different shapes with different sizes. Different objects can have the same projections on these three planes, so this method is not accurate for calculating the probabilities.

4. 2D intrusion object under gaussian distribution

In the above sections, we assume that sensor node deployment follows a uniform distribution. In this subsection, we assume that the sensor node deployment follows a two-dimensional Gaussian distribution with mean $(X/2, Y/2)$, and that the whole deployment region is denoted as $[0,X] \times [0,Y]$. Let σ denote the standard deviation, and we have the density function as follows:

$$f(x,y) = \frac{1}{2\pi\sigma^2} e^{-\frac{(x-X/2)^2+(y-Y/2)^2}{2\sigma^2}}. \quad (10)$$

We assume that a sensor node can detect an intrusion object with size o in a two-dimensional situation. We assume that the object shape is either a rectangle (with its length b and width o/b) or a circle (with $2\sqrt{o/\pi}$ as the diameter). We also assume that a sensor node's coverage area is a circle. We use Φ to denote the sensing area of a sensor node. As illustrated in Fig. 1, a sensor node's sensing range does not overlap an intrusion object if the sensor node's center is far away ($> \sqrt{\Phi/\pi}$).

We consider any random point (g,h) in the sensor network field, shown in Figs. 4 and 5, for the following two subsections, respectively. We assume that an intrusion object's central point is (g,h). Let $p(g,h)$ denote the probability that a sensor node detects an intrusion object whose central point is (g,h). $p(g,h)/k$ is the probability that the intrusion object is covered by an active sensor node. The probability that an intrusion object whose central point is (g,h) is detected by at least one active sensor node is given by

$$V_n(g,h) = 1 - [1 - p(g,h)/k]^n. \quad (11)$$

Since (g,h) is a random variable, for the intrusion detection intensity, we have

$$V_n = E(V_n(g,h)) = \int_0^X \int_0^Y V_n(g,h)\tilde{f}(g,h)dg\,dh, \quad (12)$$

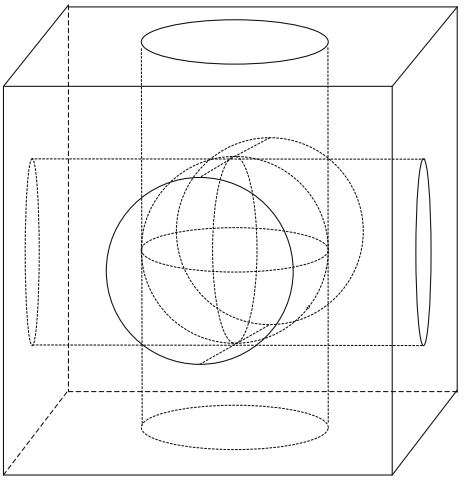

Fig. 3. An example of the projection method.

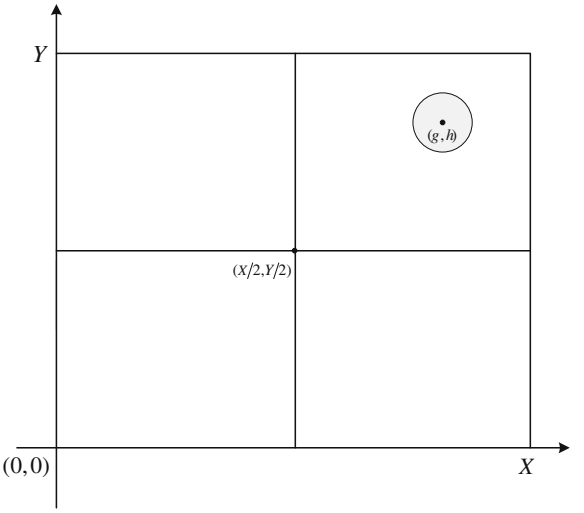

Fig. 4. 2D sensor field.

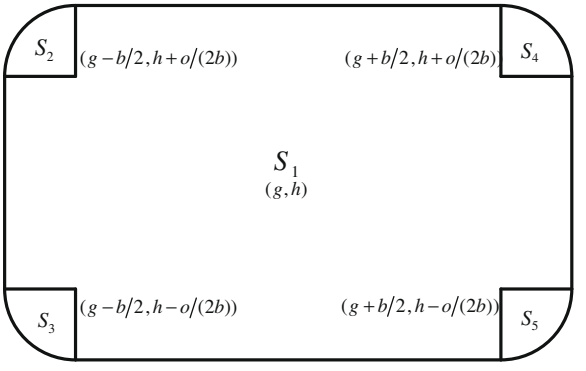

Fig. 5. Rectangle.

where $E(\cdot)$ is the mean function and $\tilde{f}(g,h)=\frac{1}{XY}$, since (g,h) is randomly chosen from the network field. Therefore, we need to derive $p(g,h)$ in the following subsections to solve (12).

4.1. Intrusion object (circle)

In this subsection, we assume that the shape of intrusion object is a circle area and then we derive the intrusion detection intensity. Because the sensing field of each sensor node is a circle with radius $\sqrt{\Phi/\pi}$, and the radius of the intrusion object is $\sqrt{o/\pi}$, a sensor node detects an intrusion object if and only if one sensor node resides in the circle centered at (g,h) with radius $\sqrt{o/\pi}+\sqrt{\Phi/\pi}$. Let r denote $\sqrt{o/\pi}+\sqrt{\Phi/\pi}$. We have

$$p(g,h)=\iint_{(x-g)^2+(y-h)^2\leqslant r^2} f(x,y)dxdy. \tag{13}$$

Let $x'=x-g$ and $y'=y-h$. We then transform (13) to

$$p(g,h)=\iint_{x'^2+y'^2\leqslant r^2}\frac{1}{2\pi\sigma^2}e^{-\frac{(x'+g-X/2)^2+(y'+h-Y/2)^2}{2\sigma^2}}dx'\,dy'. \tag{14}$$

Let $x'=l\cos\theta$ and $y'=l\sin\theta$, where $0\leqslant l\leqslant r$ and $0\leqslant\theta\leqslant 2\pi$. Let $|J|=|\frac{\partial(x,y)}{\partial(l,\theta)}|=l$, and then we can transform (12) to

$$p(g,h)=\int_0^r\int_0^{2\pi}\frac{1}{2\pi\sigma^2}e^{-\frac{(l\cos\theta+g-X/2)^2+(l\sin\theta+h-Y/2)^2}{2\sigma^2}}l\,dl\,d\theta. \tag{15}$$

4.2. Intrusion object (rectangle)

In this subsection, we assume that the shape of intrusion object is rectangular, and then we derive the intrusion detection intensity. We have

$$p(g,h)=\iint_S f(x,y)dxdy, \tag{16}$$

where $S=S_1+S_2+S_3+S_4+S_5$; S_1 is the areas of the intrusion object plus four rectangular areas, shown in Fig. 5; S_2, S_3, S_4, and S_5 are the four areas in the corners. The reasoning of Fig. 5 is the same as that of Fig. 1. Let $p_i(g,h)$ denote the portion of $p(g,h)$ in S_i $(i=1,2,3,4,5)$.

Therefore, we have

$$p(g,h)=\sum_{i=1}^{5}p_i(g,h)=\sum_{i=1}^{5}\iint_{S_i}f(x,y)dxdy. \tag{17}$$

Since the sensor node deployment follows a two-dimensional Gaussian distribution, we have

$$f(x,y)=\frac{1}{2\pi\sigma^2}e^{-[(x-X/2)^2+(y-Y/2)^2]/(2\sigma^2)}. \tag{18}$$

In the following, we derive the five parts of the probability $p(g,h)$. Since the shape of the intrusion object is a rectangle (with its length and width being b and o/b, respectively) and the sensing field of each sensor node is a circle (with radius $\sqrt{\Phi/\pi}$). Let $|J|=|\frac{\partial(x,y)}{\partial(l,\theta)}|=l, A(l,\theta,g)=l\cos\theta+g-X/2$, and $B(l,\theta,h)=l\sin\theta+h-Y/2$. We have

$$\begin{aligned}p_1(g,h)&=\iint_{S_1}f(x,y)dxdy\\&=\int_{h-o/(2b)}^{h+o/(2b)}\int_{g-b/2-\sqrt{\Phi/\pi}}^{g+b/2+\sqrt{\Phi/\pi}}f(x,y)dxdy\\&+\int_{h-o/(2b)-\sqrt{\Phi/\pi}}^{h+o/(2b)+\sqrt{\Phi/\pi}}\int_{g-b/2}^{g+b/2}f(x,y)dxdy\\&-\int_{h-o/(2b)}^{h+o/(2b)}\int_{g-b/2}^{g+b/2}f(x,y)dxdy\end{aligned}$$

$$p_2(g,h)=\int_0^{\sqrt{\Phi/\pi}}\int_{\pi/2}^{\pi}\frac{1}{2\pi\sigma^2}e^{-\frac{[A(l,\theta,g)-b/2]^2+[B(l,\theta,h)+o/(2b)]^2}{2\sigma^2}}l\,dl\,d\theta$$

$$p_3(g,h)=\int_0^{\sqrt{\Phi/\pi}}\int_{\pi}^{3\pi/2}\frac{1}{2\pi\sigma^2}e^{-\frac{[A(l,\theta,g)-b/2]^2+[B(l,\theta,h)-o/(2b)]^2}{2\sigma^2}}l\,dl\,d\theta$$

$$p_4(g,h)=\int_0^{\sqrt{\Phi/\pi}}\int_{0}^{\pi/2}\frac{1}{2\pi\sigma^2}e^{-\frac{[A(l,\theta,g)+b/2]^2+[B(l,\theta,h)+o/(2b)]^2}{2\sigma^2}}l\,dl\,d\theta$$

$$p_5(g,h)=\int_0^{\sqrt{\Phi/\pi}}\int_{3\pi/2}^{2\pi}\frac{1}{2\pi\sigma^2}e^{-\frac{[A(l,\theta,g)+b/2]^2+[B(l,\theta,h)-o/(2b)]^2}{2\sigma^2}}l\,dl\,d\theta.$$

Based on (17), we can obtain $P(g,h)$.

5. 3D intrusion object under gaussian distribution

In this subsection, we assume that the sensor node deployment follows a three-dimensional Gaussian distribution with mean $(X/2,Y/2,Z/2)$ and that the whole deployment region is denoted as $[0,X]\times[0,Y]\times[0,Z]$. We have the density function as follows:

$$f(x,y,z)=\frac{1}{(\sqrt{2\pi}\sigma)^3}e^{-\frac{(x-X/2)^2+(y-Y/2)^2+(z-Z/2)^2}{2\sigma^2}}. \tag{19}$$

We assume that a sensor node can detect an intrusion object with size o in a three-dimensional situation. We also assume that a sensor node's coverage space is a ball. We use Φ to denote the sensing space of a sensor node. As illustrated in Fig. 2, a sensor node does not overlap an intrusion object if the sensor node's center is far away $(>\sqrt[3]{3\Phi/(4\pi)})$. We consider a random point (g,h,q) in the sensor network space. We assume that an intrusion object's central point is (g,h,q). Let $p(g,h,q)$ denote the probability that a sensor node detects an intrusion object whose central point is (g,h,q).

$p(g,h,q)/k$ is the probability that an intrusion object is covered by an active sensor node. The probability that an intrusion object whose central point is (g,h,q) is detected by at least one active sensor node is given by

$$V_n(g,h,q)=1-\left[1-\frac{p(g,h,q)}{k}\right]^n \tag{20}$$

Therefore, for the intrusion detection intensity, we have

$$\begin{aligned}V_n&=E(V_n(g,h,q))\\&=\int_0^X\int_0^Y\int_0^Z V_n(g,h,q)\tilde{f}(g,h,q)dg\,dh\,dq.\end{aligned} \tag{21}$$

Since (g,h,q) is randomly chosen from the network field, we have $\tilde{f}(g,h,q)=\frac{1}{XYZ}$.

Therefore, we need to derive $p(g,h,q)$ in the following subsections to solve (21).

5.1. Intrusion object (sphere)

In this subsection, we assume that the object shape is a sphere with $\sqrt[3]{3o/(4\pi)}$ as its radius. Because the sensing space of each sensor node is a sphere with $\sqrt[3]{3\Phi/(4\pi)}$ as the radius and the radius of the intrusion object is $\sqrt[3]{3o/(4\pi)}$, a sensor node detects an intrusion object if and only if one sensor node resides in the sphere centered at (g,h,q) with radius $\sqrt[3]{3o/(4\pi)}+\sqrt[3]{3\Phi/(4\pi)}$. Let r denote $\sqrt[3]{3o/(4\pi)}+\sqrt[3]{3\Phi/(4\pi)}$. We have

$$p(g,h,q)=\iiint_{(x-g)^2+(y-h)^2+(z-q)^2\leqslant r^2} f(x,y,z)\,dx\,dy\,dz. \tag{22}$$

Let $x'=x-g, y'=y-h$ and $z'=z-q$. We then transform (22) to

$$p(g,h,q)=\iiint_{x'^2+y'^2+z'^2\leqslant r^2} \times\frac{1}{(\sqrt{2\pi}\sigma)^3}e^{-\frac{(x'+g-X/2)^2+(y'+h-Y/2)^2+(z'+q-Z/2)^2}{2\sigma^2}}dx'\,dy'\,dz' \tag{23}$$

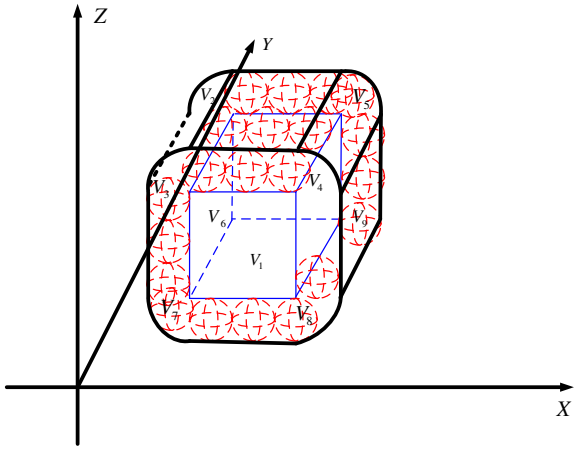

Fig. 6. Three-dimensional intrusion object emerging in the sensing space.

Let $x'=l\sin\varphi\cos\theta, y'=l\sin\varphi\sin\theta, z'=l\cos\varphi, |J|=|\frac{\partial(x,y,z)}{\partial(l,\varphi,\theta)}|=|l^2\sin\varphi|, C(l,\varphi,\theta,g)=l\sin\varphi\cos\theta+g-X/2, D(l,\varphi,\theta,h)=l\sin\varphi\sin\theta+h-Y/2$, and $F(l,\varphi,q)=l\cos\varphi+q-Z/2$, where $0\leqslant l\leqslant r$, $0\leqslant\theta\leqslant 2\pi$ and $0\leqslant\varphi\leqslant\pi$. Then we can transform (23) to

$$p(g,h,q)=\int_0^r\int_0^{2\pi}\int_0^{\pi} \times\frac{1}{(\sqrt{2\pi}\sigma)^3}e^{-\frac{C(l,\varphi,\theta,g)^2+D(l,\varphi,\theta,h)^2+F(l,\varphi,q)^2}{2\sigma^2}}|l^2 \times\sin\varphi|d\varphi\,d\theta\,dl. \tag{24}$$

5.2. Intrusion object (cuboid)

In this subsection, we assume that the object shape is cuboid. We denote its length, width, and height as b, c, and $o/(bc)$, respectively. For $p(g,h,q)$, we have

$$p(g,h,q)=\iiint_V f(x,y,z)\,dx\,dy\,dz,\quad \text{where } V=\sum_{i=1}^{9}V_i, \tag{25}$$

where V is the space of the intrusion object plus the places whose distance to the intrusion object is less than or equal to r, shown in Fig. 2. V_i is similar concept as S_i but in 3D space, shown in Fig. 6. Let $p_i(g,h,q)$ denote the portion of $p(g,h,q)$ in V_i $(i=1,\ldots,9)$.

We have

$$p(g,h,q)=\sum_{i=1}^{9}p_i(g,h,q)=\sum_{i=1}^{9}\iiint_{V_i}f(x,y,z)\,dx\,dy\,dz. \tag{26}$$

Since the sensor node deployment follows a three-dimensional Gaussian distribution, we have

$$f(x,y,z)=\frac{1}{(\sqrt{2\pi}\sigma)^3}e^{-[(x-X/2)^2+(y-Y/2)^2+(z-Z/2)^2]/(2\sigma^2)}.$$

Assume that three edges of the object are parallel to the x-axis, the y-axis, and z-axis, respectively. We have

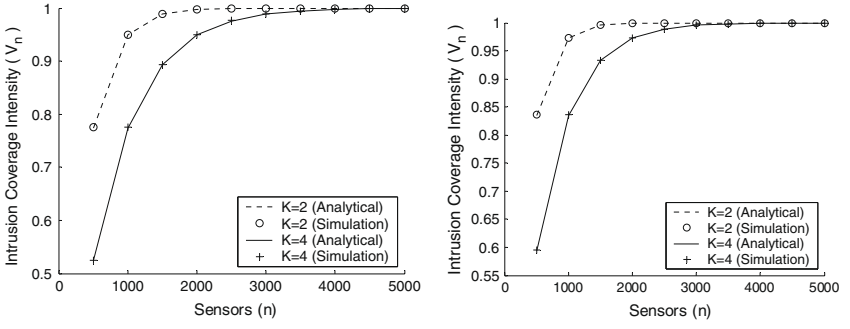

(a) V_n vs. Number of Sensor Nodes: circular object (b) V_n vs. Number of Sensor Nodes: rectangular object

Fig. 7. Intrusion coverage intensity vs. number of sensor nodes.

$$
\begin{aligned}
P_1(g,h,q) &= \iiint_{V_1} f(x,y,z)dx\,dy\,dz = \int_{q-o/(2bc)-\sqrt[3]{3\Phi/(4\pi)}}^{q+o/(2bc)+\sqrt[3]{3\Phi/(4\pi)}} \int_{h-c/2}^{h+c/2} \int_{g-b/2}^{g+b/2} f(x,y,z)dx\,dy\,dz \\
&+ \int_{q-o/(2bc)}^{q+o/(2bc)} \int_{h-c/2-\sqrt[3]{3\Phi/(4\pi)}}^{h+c/2+\sqrt[3]{3\Phi/(4\pi)}} \int_{g-b/2}^{g+b/2} f(x,y,z)dx\,dy\,dz \\
&+ \int_{q-o/(2bc)}^{q+o/(2bc)} \int_{h-c/2}^{h+c/2} \int_{g-b/2-\sqrt[3]{3\Phi/4\pi}}^{g+b/2+\sqrt[3]{3\Phi/4\pi}} f(x,y,z)dx\,dy\,dz \\
&- 2\int_{q-o/(2bc)}^{q+o/(2bc)} \int_{h-c/2}^{h+c/2} \int_{g-b/2}^{g+b/2} f(x,y,z)dx\,dy\,dz,
\end{aligned}
$$

$$
\begin{aligned}
P_2(g,h,q) &= \int_0^{\sqrt[3]{3\Phi/(4\pi)}} \int_{\pi/2}^{\pi} \int_0^{\pi/2} \frac{1}{(\sqrt{2\pi}\sigma)^3} e^{-\frac{[C(l,\varphi,\theta,g)-b/2]^2+[D(l,\varphi,\theta,h)+c/2]^2+[F(l,\varphi,q)+o/(2bc)]^2}{2\sigma^2}} |J|d\varphi\,d\theta\,dl, \\
P_3(g,h,q) &= \int_0^{\sqrt[3]{3\Phi/(4\pi)}} \int_{\pi}^{3\pi/2} \int_0^{\pi/2} \frac{1}{(\sqrt{2\pi}\sigma)^3} e^{-\frac{[C(l,\varphi,\theta,g)-b/2]^2+[D(l,\varphi,\theta,h)-c/2]^2+[F(l,\varphi,q)+o/(2bc)]^2}{2\sigma^2}} |J|d\varphi\,d\theta\,dl, \\
P_4(g,h,q) &= \int_0^{\sqrt[3]{3\Phi/(4\pi)}} \int_{3\pi/2}^{2\pi} \int_0^{\pi/2} \frac{1}{(\sqrt{2\pi}\sigma)^3} e^{-\frac{[C(l,\varphi,\theta,g)+b/2]^2+[D(l,\varphi,\theta,h)-c/2]^2+[F(l,\varphi,q)+o/(2bc)]^2}{2\sigma^2}} |J|d\varphi\,d\theta\,dl, \\
P_5(g,h,q) &= \int_0^{\sqrt[3]{3\Phi/(4\pi)}} \int_0^{\pi/2} \int_0^{\pi/2} \frac{1}{(\sqrt{2\pi}\sigma)^3} e^{-\frac{[C(l,\varphi,\theta,g)+b/2]^2+[D(l,\varphi,\theta,h)+c/2]^2+[F(l,\varphi,q)+o/(2bc)]^2}{2\sigma^2}} |J|d\varphi\,d\theta\,dl, \\
P_6(g,h,q) &= \int_0^{\sqrt[3]{3\Phi/(4\pi)}} \int_{\pi/2}^{\pi} \int_{\pi/2}^{\pi} \frac{1}{(\sqrt{2\pi}\sigma)^3} e^{-\frac{[C(l,\varphi,\theta,g)-b/2]^2+[D(l,\varphi,\theta,h)+c/2]^2+[F(l,\varphi,q)-o/(2bc)]^2}{2\sigma^2}} |J|d\varphi\,d\theta\,dl, \\
P_7(g,h,q) &= \int_0^{\sqrt[3]{3\Phi/(4\pi)}} \int_{\pi}^{3\pi/2} \int_{\pi/2}^{\pi} \frac{1}{(\sqrt{2\pi}\sigma)^3} e^{-\frac{[C(l,\varphi,\theta,g)-b/2]^2+[D(l,\varphi,\theta,h)-c/2]^2+[F(l,\varphi,q)-o/(2bc)]^2}{2\sigma^2}} |J|d\varphi\,d\theta\,dl, \\
P_8(g,h,q) &= \int_0^{\sqrt[3]{3\Phi/(4\pi)}} \int_{3\pi/2}^{2\pi} \int_{\pi/2}^{\pi} \frac{1}{(\sqrt{2\pi}\sigma)^3} e^{-\frac{[C(l,\varphi,\theta,g)+b/2]^2+[D(l,\varphi,\theta,h)-c/2]^2+[F(l,\varphi,q)-o/(2bc)]^2}{2\sigma^2}} |J|d\varphi\,d\theta\,dl, \\
P_9(g,h,q) &= \int_0^{\sqrt[3]{3\Phi/(4\pi)}} \int_0^{\pi/2} \int_{\pi/2}^{\pi} \frac{1}{(\sqrt{2\pi}\sigma)^3} e^{-\frac{[C(l,\varphi,\theta,g)+b/2]^2+[D(l,\varphi,\theta,h)+c/2]^2+[F(l,\varphi,q)-o/(2bc)]^2}{2\sigma^2}} |J|d\varphi\,d\theta\,dl,
\end{aligned}
\tag{27}
$$

where $|J| = |\frac{\partial(x,y,z)}{\partial(l,\varphi,\theta)}| = |l^2 \sin\varphi|$.

6. Performance evaluation

In this section, we evaluate the performance of different intrusion detection scenarios, including both 2D and 3D situations. We mainly focus on factors that influence the detection intensity, as well as the impact of object size on the deployment of sensor networks. Such studies are helpful in the deployment of sensor networks especially when the kind of intrusion objects, such as the size of objects, is of interest.

6.1. Performance evaluation with a 2D intrusion object

In this subsection, we study the performance of detection probability and intrusion coverage intensity via both simulation and analytical results. All of the results consider both the circular intrusion objects and the rectangular intrusion objects. Simulations were conducted with discrete event simulation using C++.

6.1.1. Intrusion coverage intensity

We study the performance of intrusion coverage intensity versus number of sensor nodes, number of subsets, and object size.

Fig. 7 shows the performance of intrusion coverage intensity with parameters as follows: $k = 2$ or 4, $a = 10{,}000$, $\Phi = 30$, and $o = 5$. Both analytical results and simulation results are studied. Fig. 7a shows the performance with a circular intrusion object, and from the figure we observe that the intrusion coverage intensity increases as the number of nodes increases. A larger k corresponds to decreased intrusion coverage intensity. From (3), we know that a large n will lead to high intrusion coverage intensity, and that when n goes to infinity, the coverage intensity runs to 1. Fig. 7b shows the similar performance of intrusion coverage intensity with a rectangular intrusion object (5 by 1 rectangle). In both Fig. 7a and b, the analytical results match the simulation results nicely.

In Fig. 8, simulations are conducted with $n = 5000$ and $n = 3000$, while $a = 10{,}000$, $\Phi = 30$, and $o = 5$. Both analytical results and simulation results are studied. Fig. 8a shows the performance with a circular intrusion object, and from the figure we observe that the intrusion coverage intensity decreases as the number of subsets increases. When k goes to infinity, the intrusion coverage intensity runs to 0. From (3), we know that intrusion coverage intensity is a decreasing function of k, and a larger n corresponds to higher coverage intensity. Fig. 8b shows the similar performance of intrusion coverage intensity with a rectangular intrusion object (5 by 1 rectangle). In both Fig. 8a and b, the analyt-

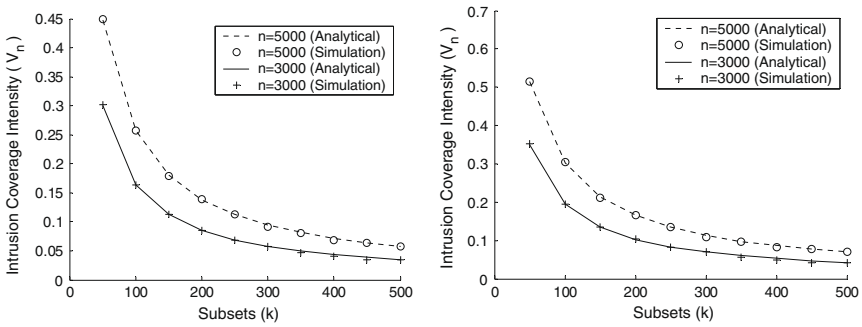

(a) V_n vs. Number of Subsets: circle object (b) V_n vs. Number of Subsets: rectangular object

Fig. 8. Intrusion coverage intensity vs. number of subsets.

ical results match the simulation results nicely. Normally, we would not divide the sensor nodes into so many subsets. However, for a deeper understanding of subsets (k), we take a broad range to see the impacts of number of subsets.

In Fig. 9, parameters are chosen as $k = 2$ or 4, $n = 1000$, $a = 10{,}000$ and $\Phi = 30$. Both analytical results and simulation results are studied. Fig. 9a and b shows the performance with a circular intrusion object and with a rectangular intrusion object (with one pair of sides fixed at 5 and another pair of sides varying), respectively. Both figures show a similar performance of intrusion coverage intensity. By intuition, the intrusion coverage intensity increases as the intrusion object size increases, and this is illustrated in the figures. A larger k makes the coverage intensity lower. In both Fig. 9a and b, the analytical results match the simulation results nicely.

Fig. 9c shows the performance of intrusion coverage intensity vs. object length b of a rectangular intrusion object, where $o = 25$ and $n = 500$. As illustrated in the figure, the intrusion coverage intensity first decreases and then increases as b increases. We observe from the figure that, when $b = \sqrt{o}$, the intrusion coverage intensity reaches its minimum value. That is because p_1 reaches its minimum value when $b = \sqrt{o}$. This confirms Lemma 5. Intuitively, the lowest intrusion coverage intensity should correspond

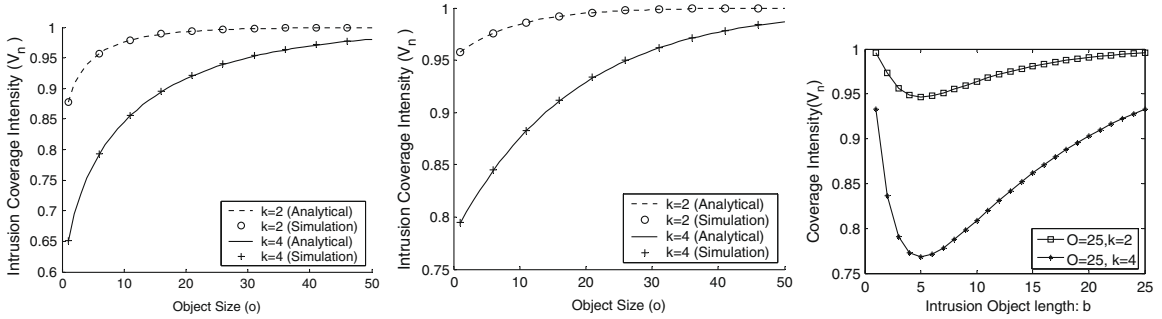

(a) Vn vs.Number of Object Size: circle object (b) Vn vs. Object Size: rectangular object (c) Vn vs. Intrusion object length: rectangular object.

Fig. 9. Intrusion coverage intensity vs. object size.

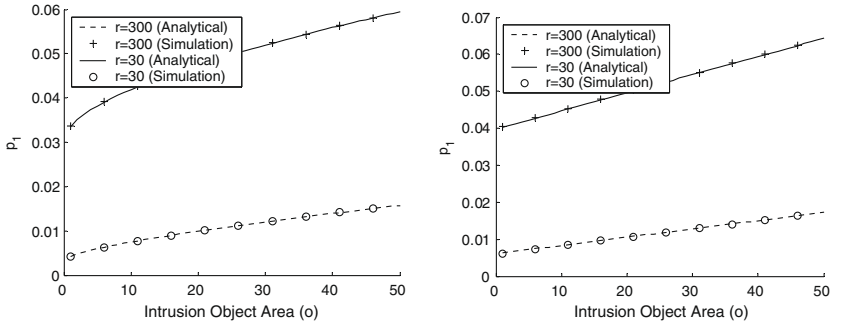

(a) p_1 vs. Intrusion Object area: circular object (b) p_1 vs. Intrusion Object Area: rectangular object

Fig. 10. Detection probability vs. intrusion object area.

to the smallest intrusion object size. Note that the *x*-axis is not the size of the intrusion object, but its *b* value.

6.1.2. Detection probability

Fig. 10 shows the performance of detection probability while $a = 10{,}000$ and $n = 1000$. Both analytical results and simulation results are studied. Fig. 10a shows the performance with a circular intrusion object, and Fig. 10b shows the performance with a rectangular object (with one pair of sides fixed at 5 and another pair of sides varying). As illustrated in the figures, the detection probability increases as the size of the intrusion objects increases, and a larger Φ corresponds to a larger detection probability. This is also consistent with our intuition. In both Fig. 10a and b, the analytical results match the simulation results nicely.

6.1.3. Sensor network deployment

Fig. 11a shows the sensor node deployment for a circular object, where $a = 10{,}000$, $\Phi = 30$, and $k = 4$. As illustrated in the figure, the minimum number of sensor nodes required decreases as the size of the intrusion object increases. Higher intrusion coverage intensity requires more sensor nodes. Fig. 11b shows a similar result as in Fig. 11a, with the circular intrusion object. The figures answer Question A in the above.

Fig. 11c shows the impact of *object length* of a rectangular intrusion object, where $a = 10{,}000$, $\Phi = 30$ and $k = 4$. The object size is fixed at 25. As illustrated in the figure, the required n value reaches its peak at $b = \sqrt{a}$.

Fig. 12a shows the required maximum k value (i.e., the number subsets) when parameters are chosen as $a = 10{,}000$, $\Phi = 30$, and $n = 3000$. As illustrated in the

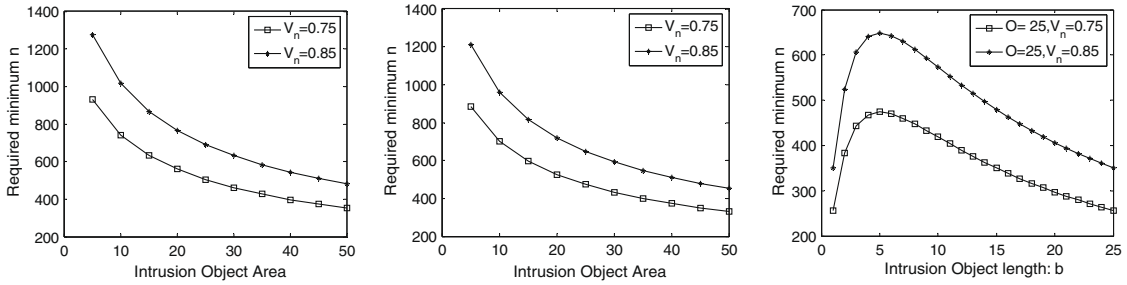

(a) Required minimum n vs. object area: circle object (b) Required minimum n vs. object area: rectangular object (c) Required minimum n vs. b: rectangular object

Fig. 11. Required minimum n vs. object area.

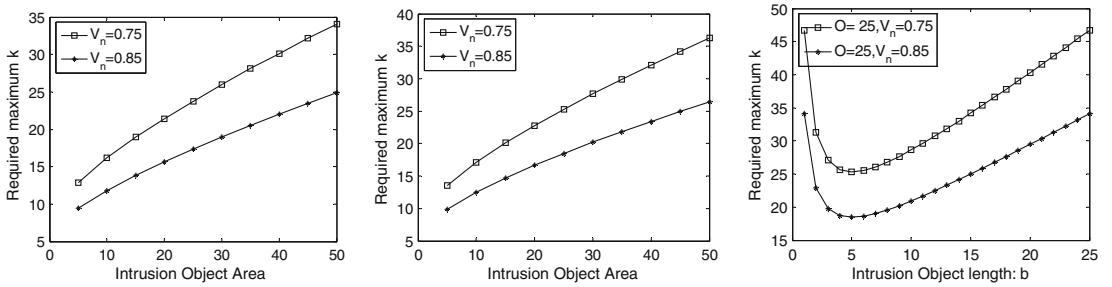

(a) Required maximum k vs. object area: circle object (b) Required maximum k vs. object area: rectangular object (c) Required maximum k vs. b: rectangle object

Fig. 12. Required maximum k vs. intrusion object area.

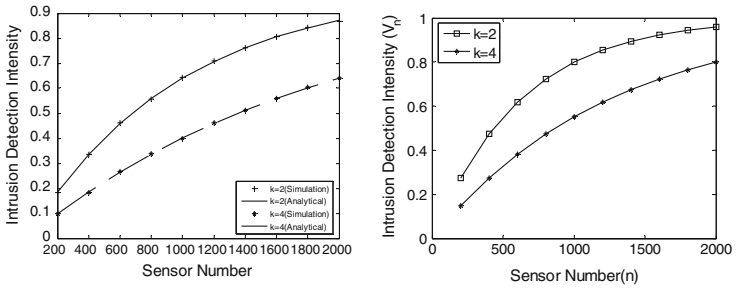

(a) V_n vs. Number of Sensor Nodes: spherical object (b) V_n vs. Number of Sensor Nodes: cuboid object

Fig. 13. Intrusion detection intensity vs. number of sensor nodes.

figure, the required maximum number of subsets increases as the size of the intrusion object increases. Higher intrusion coverage intensity requires a smaller k. Fig. 12b shows a similar result as in Fig. 12a, with the circular intrusion object. The figures answer Question B in the above.

Fig. 12c shows the impact of *object length* of a rectangular intrusion object, where $a = 10{,}000$, $\Phi = 30$ and $n = 3000$. The object size is 25. As illustrated in the figure, the required k value reaches its peak at $b = \sqrt{o}$.

6.2. Performance evaluation with a 3D intrusion object

In this subsection, we study the performance of detection probability and intrusion detection intensity via both simulations and analytical results. All of the results consider both the spherical intrusion objects and cuboid intrusion objects.

6.2.1. Intrusion detection intensity

We study the performance of intrusion detection intensity versus the number of sensor nodes, number of subsets, and object size.

In Fig. 13, simulations are conducted with parameters chosen as $k = 2$ or 4, $a = 1{,}000{,}000$, $\Phi = 500$, and o(*object size*) = 100. Fig. 13a shows the performance with a spherical intrusion object. Both the analytical results and simulation results are studied and from the figure we observe that the intrusion detection intensity increases as the number of nodes increases. A larger k corresponds to lower intrusion detection intensity. From (2), we know that a large n will lead to high intrusion detection intensity, and that when n goes to infinity, the detection intensity runs to 1. In Fig. 13a, the analytical results match the simulation results nicely. Fig. 13b shows the similar performance of intrusion detection intensity with a cuboid intrusion object ($o = 100$, $c = 15$, $b = 5$).

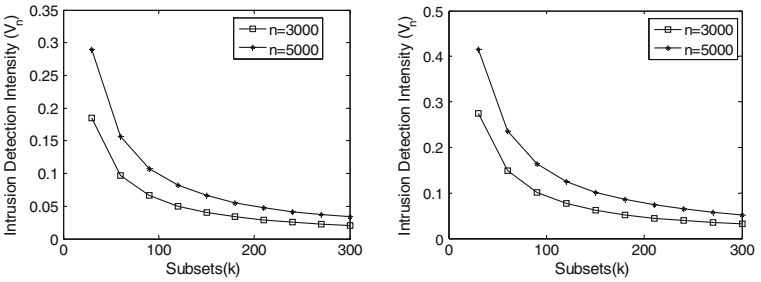

(a) V_n vs. Number of Subsets: spherical object (b) V_n vs. Number of Subsets: cuboid object

Fig. 14. Intrusion detection intensity vs. number of subsets.

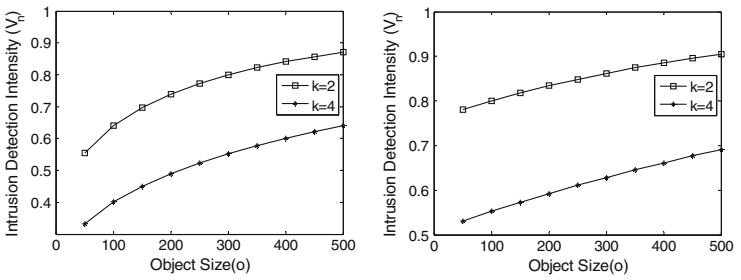

(a) V_n vs.Object Size: spherical object (b) V_n vs. Object Size: cuboid object

Fig. 15. Intrusion detection intensity vs. object size.

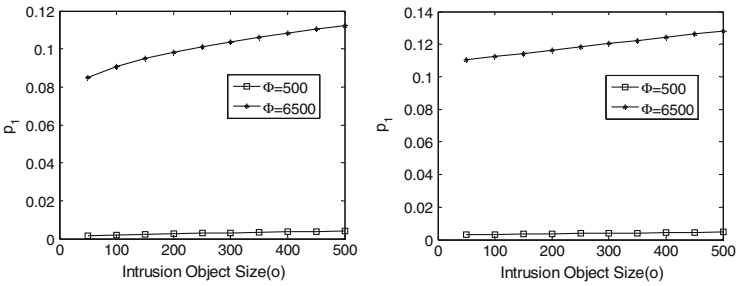

(a) p_1 vs. Intrusion Object Size: spherical object (b) p_1 vs. Intrusion Object Size: cuboid object

Fig. 16. Detection probability vs. intrusion object size.

In Fig. 14, parameters are chosen as $n = 5000$ or 3000, $a = 1{,}000{,}000$, $\Phi = 500$, and $o = 100$. Fig. 14a shows the performance with a spherical intrusion object, and from the figure we observe that the intrusion detection intensity decreases as the number of subsets increases. When k goes to infinity, the intrusion detection intensity runs to 0. From (3), we know that intrusion detection intensity is a decreasing function of k, and that a larger n corresponds to higher intrusion detection intensity. Fig. 14b shows the similar performance of intrusion detection intensity with a cuboid intrusion object ($o = 100$, $c = 15$, $b = 5$). Normally, we would not divide the sensor nodes into so many subsets. However, for a deeper understanding of subsets (k), we take a broad range to see the impacts of the number of subsets.

Fig. 15 shows the performance of intrusion detection intensity with parameters as follows: $k = 2$ or $k = 4$, $n = 1000$, $a = 1{,}000{,}000$ and $\Phi = 500$. Fig. 15a and b shows the performance with a spherical intrusion object and with a cuboid intrusion object (with one pair of sides fixed at 5, 15 and the third side varying), respectively. Both figures show the similar performance of intrusion detection intensity. By intuition, the intrusion detection intensity increases as the size of the intrusion object increases, and this is also illustrated in the figures. A larger k makes the detection intensity lower.

6.2.2. Detection probability

Fig. 16 shows the performance of detection probability with $a = 1{,}000{,}000$. Fig. 16a shows the performance with a spherical intrusion object, and Fig. 16b shows the performance with a cuboid object (with one pair of sides fixed at 5, 15 and the third side varying). As illustrated in the figures, the detection probability increases as the size of the intrusion objects increases, and a larger Φ corresponds to a larger detection probability. This is also consistent with our intuition.

6.2.3. Sensor network deployment

Fig. 17a shows the required minimum number of sensor nodes for a given intrusion detection intensity with a spherical intrusion object when $a = 1{,}000{,}000$, $\Phi = 500$, and $k = 4$. As illustrated in the figure, the minimum number of sensor nodes required decreases as the size of the intrusion object increases. Higher intrusion detection intensity requires more sensor nodes. Fig. 17b shows a similar result as in Fig. 17a, with the intrusion object being cuboid. The figures answer Question A in the above.

Fig. 18a shows the required maximum k value (i.e., the number of subsets) for a given detection intensity with a spherical intrusion object when $a = 1{,}000{,}000$, $\Phi = 500$, and $n = 3000$. As illustrated in the figure, the maximum number of subsets required increases as the size of the intrusion object increases. A higher intrusion detection intensity needs a smaller k. Fig. 18b shows the similar result as in Fig. 18a while the intrusion object is represented as a cuboid. The figures answer Question B in the above.

6.3. Asymptotic coverage and other properties

Fig. 19a shows $V(m)$ over m. As illustrated in the figure, $V(m)$ increases exponentially as m increases and goes to 1 as m goes to infinity. Fig. 19b shows $V(m)$ over p_1. As illustrated in the figure, $V(m)$ increases exponentially as p_1 increases and goes to 1 as p_1 goes to infinity.

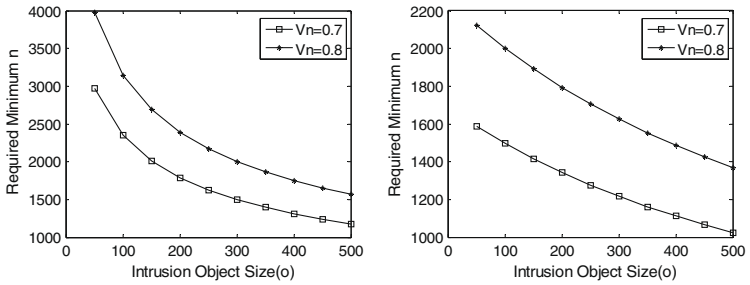

(a) Required Minimum n vs. ObjectSize: spherical object (b) Required minimum n vs. Object Size: cuboid object

Fig. 17. Required minimum n vs. object size.

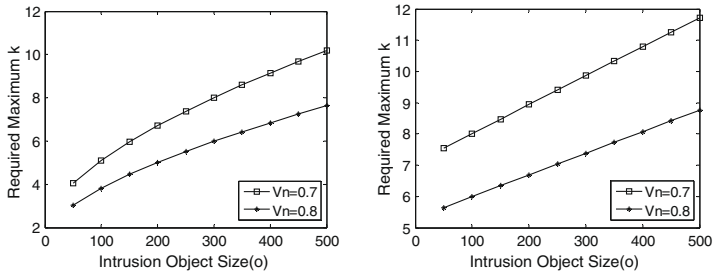

(a) Required maximum k vs. Object Size: spherical object (b) Required maximum k vs. Object Size: cuboid object

Fig. 18. Required maximum k vs. intrusion object size.

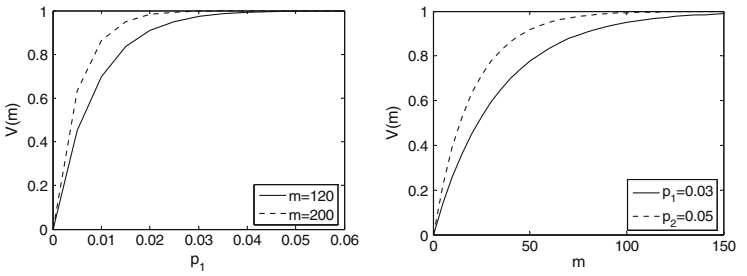

(a) $V(m)$ vs. m (b) $V(m)$ vs. p_1

Fig. 19. Asymptotic coverage.

6.4. Intrusion coverage intensity under gaussian distribution

In this subsection, we study the performance of intrusion coverage intensity versus the number of sensor nodes and the number of subsets when the deployment of sensor nodes follows Gaussian distribution.

6.4.1. Performance evaluation with a 2D intrusion object

Fig. 20 shows the performance of intrusion coverage intensity vs. the number of sensor nodes for different numbers of subsets ($k = 2$ and $k = 4$) when $a = 10{,}000$ ($X = 100$, $Y = 100$), $\Phi = 30$, $o = 5$, and the standard deviation of Gaussian distribution σ is 15. Fig. 20a shows the performance with a circular object. As illustrated in Fig. 20a, the intrusion coverage intensity increases as the number of nodes increases. A larger k corresponds to lower intrusion coverage intensity and a larger n leads to higher intrusion coverage intensity. When n goes to infinity, the intrusion coverage intensity goes to 1. Fig. 20b shows the similar performance of intrusion coverage intensity with a rectangular intrusion object (5 by 1 rectangle).

Fig. 21 shows the performance of intrusion coverage intensity vs. the number of subsets for different numbers of sensor nodes ($n = 5000$ and $n = 3000$) when $a = 10{,}000$ ($X = 100$, $Y = 100$), $\Phi = 30$, $o = 5$, and the standard deviation of Gaussian distribution σ is 15. Fig. 21a shows the performance with a circular object. As illustrated in Fig. 21a, the intrusion coverage intensity decreases as the number of subsets increases; when k goes to infinity, the coverage intensity goes to 0; and a larger n corresponds to higher intrusion coverage intensity. Fig. 21b shows the similar performance of intrusion coverage intensity with a rectangular intrusion object (5 by 1 rectangle).

6.4.2. Performance evaluation with a 3D intrusion object

Fig. 22 shows the performance of intrusion coverage intensity vs. the number of sensor nodes for different number of subsets ($k = 2$ and $k = 4$), where the intrusion object is a spherical object. The parameters are chosen as

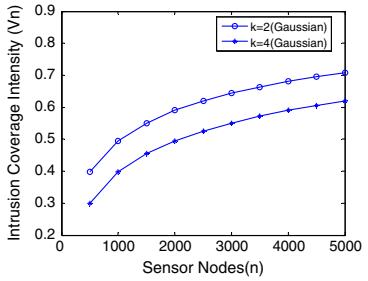

(a) V_n vs. Number of Sensor Nodes: circular object

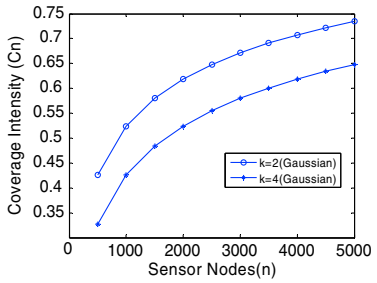

(b) V_n vs. Number of Sensor Nodes: rectangular object

Fig. 20. Intrusion coverage intensity vs. number of sensor nodes (Gaussian).

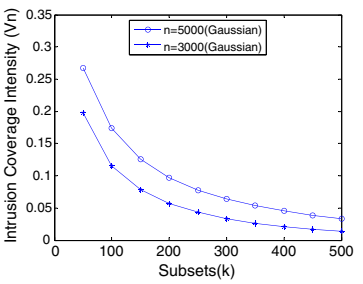

(a) V_n vs. Number of Subsets: circular object

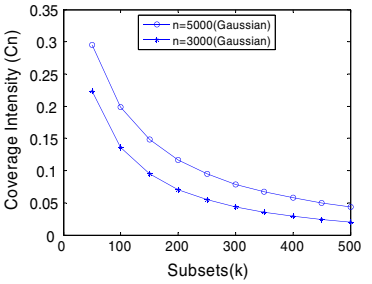

(b) V_n vs. Number of Subsets: rectangular object

Fig. 21. Intrusion coverage intensity vs. number of subsets (Gaussian).

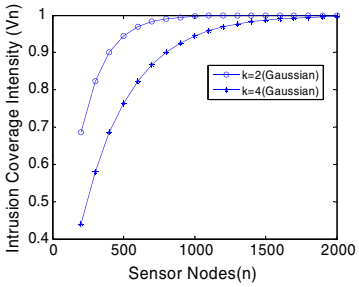

(a) Vn vs. Number of Sensor Nodes: spherical object whose central point is (70,66,68)

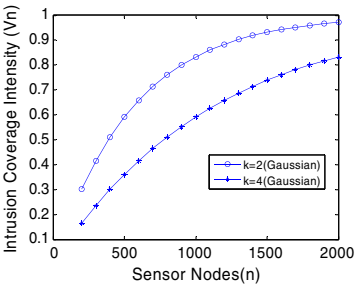

(b) Vn vs. Number of Sensor Nodes: spherical object whose central point is (76,72,70)

Fig. 22. Intrusion detection intensity vs. number of sensor nodes: spherical object.

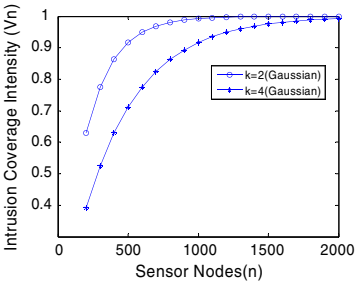

(a) V_n vs. Number of Sensor Nodes: cuboid object whose central point is (66,62,60)

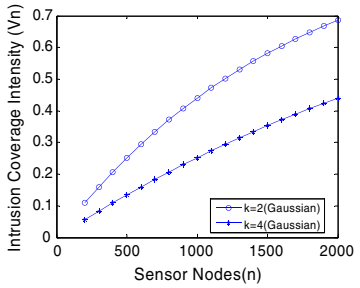

(b) V_n vs. Number of Sensor Nodes: cuboid object whose central point is (76,72,70)

Fig. 23. Intrusion detection intensity vs. number of sensor nodes: cuboid object.

a = 1,000,000 (X = 100, Y = 100, Z = 100), Φ = 500, o(*object size*) = 100, and the standard deviation of Gaussian distribution σ is 15. Fig. 22a shows the performance of a particular spherical object whose central point is (70, 66, 68). As illustrated in Fig. 22a, the intrusion coverage intensity increases as the number of nodes increases. A larger k corresponds to lower intrusion coverage intensity and a larger n will lead to higher intrusion coverage intensity. When n goes to infinity, the intrusion coverage intensity goes to 1. Fig. 22b shows the similar performance of intrusion coverage intensity with a particular spherical intrusion object whose central point is (76, 72, 70). By comparing Fig. 22a with b, we can observe that the intrusion detection intensity of object centered at (70, 66, 68) is larger than object centered at (76, 72, 70). This fact reflects that the sensor node has a high probability to reside around the central deployment area under Gaussian distribution.

Fig. 23 shows the performance of intrusion coverage intensity vs. the number of sensor nodes for different number of subsets (k = 2 and k = 4), where the intrusion object is a cuboid object. The parameters are chosen as a = 1,000,000 (X = 100, Y = 100, Z = 100), Φ = 500, o(*object size*) = 100, c = 15, b = 5, and the standard deviation of Gaussian distribution σ is 15. Fig. 23a shows the performance of a particular cuboid object whose central point is (66, 62, 60). As illustrated in Fig. 23a, the intrusion coverage intensity increases as the number of nodes increases. A larger $k$corresponds to lower intrusion coverage intensity and a larger n will lead to higher intrusion coverage intensity. When n goes to infinity, the intrusion coverage intensity goes to 1. Fig. 23b shows the similar performance of intrusion coverage intensity with a particular cuboid intrusion object whose central point is (76, 72, 70). By comparing Fig. 23a with b, we can also observe that the intrusion detection intensity of object centered at (66, 62,60) is larger than object centered at (76, 72, 70). This fact also reflects that the sensor node has a high probability to reside around the central deployment area under Gaussian distribution.

7. Conclusion

Energy saving and network lifetime are important topics for wireless sensor networks, and the k-set randomized scheduling algorithm extends the lifetime of the network. In this paper, we studied the intrusion detection problem in the sensor network from a static and statistical view, and we evaluated the performance of the randomized scheduling algorithms with intrusion objects occupying two-dimensional areas or three-dimensional spaces. In addition, we studied the sensor network deployment in more realistic settings. For example, we studied the cases in which the deployments of sensor nodes follow two-dimensional and three-dimensional Gaussian distributions in a two-dimensional plane and a three-dimensional space, respectively. Multiple performance metrics such as detection probability and intrusion coverage intensity were studied via both computer simulations and mathematical analysis. The detection probability and the coverage intensity were studied while varying the object size, the number of sensor nodes, the sensing radius, the number of subsets, and the size of the monitored region. In addition, we studied the influence of the sizes and shapes of the intrusion objects on sensor network's configuration. Our results provide us

with a guideline of how a sensor network can be set up to meet a certain detection capability to detect practical objects, such as enemy tanks in more realistic settings.

Acknowledgements

This work is supported in part by the US National Science Foundation (NSF) under the Grant Numbers CCF-0829827, CNS-0716211, and CNS-0737325. Xiaojiang Du's research is supported in part by the US NSF under the grant numbers CNS-0721907 and CNS-0709268, as well as the Army Research Office under Grants W911NF-07-1-0250 and W911NF-08-1-0334. Bo Sun's research is supported in part by the US NSF under the grant number DUE-0633445. Kui Wu's research was partially supported by Natural Sciences and Engineering Research Council of Canada (NSERC) and Canada Foundation for Innovation (CFI).

References

[1] Z. Abrams, A. Goel, S. Plotkin, Set *k*-cover algorithms for energy efficient monitoring in WSNs, in: Proceedings of IPSN, 2004.
[2] C. Hsin, M. Liu, Network coverage using low duty-cycled sensors: random and coordinated sleep algorithm, in: Proceedings of IPSN, 2004.
[3] S. Meguerdichian, F. Koushanfar, M. Potkonjak, M. Srivastava, Coverage problems in wireless ad-hoc sensor networks, in: Proceedings of IEEE INFOCOM, 2001.
[4] D. Tian, D. Georganas, A coverage-preserving node scheduling scheme for large WSNs, in: Proceedings of WSNA, 2002.
[5] K. Wu, Y. Gao, F. Li, Y. Xiao, Lightweight deployment-aware scheduling for WSNs, ACM/Springer Mobile Networks and Applications (MONET), Special Issue on Energy Constraints and Lifetime Performance in WSNs 10(6) (2005) 837–852.
[6] T. Yan, T. He, J. Stankovic, Differentiated surveillance for sensor networks, in: Proceedings of ACM SenSys, 2003.
[7] F. Ye, G. Zhong, J. Cheng, S. Lu, L. Zhang, Peas: a robust energy conserving protocol for long-lived sensor networks, in: Proceedings of ICNP, 2002.
[8] L. Wang, Y. Xiao, A survey of energy-efficient scheduling mechanisms in sensor networks, ACM/Springer Mobile Networks and Applications (MONET) 11 (5) (2006) 723–740.
[9] C. Liu, K. Wu, Y. Xiao, B. Sun, Random coverage with guaranteed connectivity: joint scheduling for WSNs, IEEE Transactions on Parallel and Distributed Systems 17 (6) (2006) 562–575.
[10] Y. Xiao, H. Chen, K. Wu, C. Liu, B. Sun, Maximizing network life time under QoS constraints in WSNs, in: Proceedings of GLOBECOM, 2006.
[11] Y. Xiao, H. Chen, K. Wu, B. Sun, Modeling detection metrics in randomized scheduling algorithm in wireless sensor networks, in: Proceedings of IEEE WCNC, 2007.
[12] B. Chen, K. Jamieson, H. Balakrishnan, R. Morris, Span: an energy-efficient coordination algorithm for topology maintenance in ad hoc wireless networks, in: Proceedings of Mobicom, 2001.
[13] E. Elson, K. Romer, Wireless sensor networks: a new regime for time synchronization, in: Proceedings of First Workshop on Hot Topics in Networks, Princeton, New Jersey, October 2002.
[14] P. Godfrey, D. Ratajczak, Naps: scalable, robust topology management in wireless ad hoc networks, in: Proceedings of IPSN, 2004.
[15] H. Gupta, S. Das, Q. Gu, Connected sensor cover: self-organization of sensor networks for efficient query execution, in: Proceedings of MobiHoc, 2003.
[16] S. Ren, Q. Li, H. Wang, X. Chen, X. Zhang, Design and analysis of sensing scheduling algorithms under partial coverage for object detection in sensor networks, IEEE Transactions on Parallel and Distributed Systems 18 (3) (2007).
[17] C. Schurgers, V. Tsiatsis, S. Ganeriwal, M. Strivastava, Topology management for sensor networks: exploiting latency and density, in: Proceedings of MobiHoc, 2002.
[18] S. Shakkottai, R. Srikant, N. Shroff, Unreliable sensor grids: coverage, connectivity and diameter, in: Proceedings of INFOCOM, 2003.
[19] S. Slijepcevic, M. Potkonjak, Power efficient organization of WSNs, in: Proceedings of ICC, 2001.
[20] S. Tilak, N. Abu-Ghazaleh, W. Heinzelman, Infrastructure tradeoffs for sensor networks, in: Proceedings of WSNA'02.
[21] X. Wang, G. Xing, Y. Zhang, C. Lu, R. Pless, C. Gill, Integrated coverage and connectivity configuration in WSNs, in: Proceedings of Sensys, 2003.
[22] H. Zhang, J. Hou, Maintaining coverage and connectivity in large sensor networks, in: Proceedings of WTASA, 2004.
[23] I. Akyildiz, W. Su, Y. Sankarasubramaniam, E. Cayirci, Survey on sensor networks, IEEE Communications Magazine 40 (8) (2002) 102–114.
[24] Y. Xiao, Y. Zhang, X. Sun, H. Chen, Asymptotic coverage and detection in randomized scheduling algorithm in wireless sensor networks, in: Proceedings of IEEE ICC, 2007.
[25] I.F. Akyildiz, W. Su, Y. Sankarasubramaniam, E. Cayirci, A survey on sensor networks, IEEE Communications Magazine (August) (2002) 102–114.
[26] D. Culler, D. Estrin, M. Srivastava, Overview of sensor networks, IEEE Computer magazine (August) (2004) 41–49.
[27] M. Ilyas, I. Mahgoub, Handbook of Sensor Networks: Compact Wireless and Wired Sensing Systems, CRC Press, 2004.
[28] Olivier Dousse, Christina Tavoularis, Patrick Thiran, Delay of intrusion detection in wireless sensor networks, in: Proceedings of the Seventh ACM International Symposium on Mobile Ad hoc Networking and Computing, May 22–25, 2006, Florence, Italy.
[29] C. Gui, P. Mohapatra, Power conservation and quality of surveillance in target tracking sensor networks, in: Proceedings of Mobicom, Philadelphia, September 2004.
[30] T. He et al., Energy-efficient surveillance system using wireless sensor networks, in: Proceedings of MobiSYS, Boston, MA, June 2004.
[31] S. Pattem, S. Poduri, B. Krishnamachari, Energy-quality tradeoffs for target tracking in wireless sensor networks, in: Proceedings of ISPN'03, April 2003.
[32] E.B. Ermis, V. Saligrama, Detection and localization in sensor networks using distributed FDR, in: Proceedings of the 40th Conference on Information Science and Systems Princeton.
[33] Y. Xu, Energy-Aware Object Tracking Sensor Networks, <http://www.cse.msu.edu/icdcs/doctoral/yixu.pdf>.
[34] D.R.Thompson, D. Wettergreen, Multiple-object detection in natural scenes with multiple-view expectation maximization clustering, in: IEEE/RSJ International Conference on Intelligent Robots and Systems, August 2005, pp. 448–453.
[35] K. Mechitov, S. Sundresh, Y. Kwon, Cooperative Tracking with Binary-Detection Sensor Networks, Technical Report UIUCDCS-R-2003-2379, Univ. of Illinois at Urbana-Champaign, 2003.
[36] C.M. Bishop, Neural Networks for Pattern Recognition, Oxford U. P., Oxford, 1995.
[37] A.P. Dempster, N.M. Laird, D.B. Rubin, Maximum likelihood from incomplete data via the em algorithm, Journal of the Royal Statistical Society 39 (1997) 1–38.
[38] Y. Xiao, Editorial, International Journal of Sensor Networks 1 (1/2) (2006) 1.
[39] M.-S. Pan, C.-H. Tsai, Y.-C. Tseng, Emergency guiding and monitoring applications in indoor 3D environments by wireless sensor networks, International Journal of Sensor Networks 1 (1/2) (2006) 2–10.
[40] M. Ma, Y. Yang, C. Ma, Single-path flooding chain routing in mobile wireless networks, International Journal of Sensor Networks 1 (1/2) (2006) 11–19.
[41] F. Ovalle-Martínez, A. Nayak, I. Stojmenovic, J. Carle, D. Simplot-Ryl, Area-based beaconless reliable broadcasting in sensor networks, International Journal of Sensor Networks 1 (1/2) (2006) 20–33.
[42] J. Misic, S. Shafi, V.B. Misic, Real-time admission control in 802.15.4 sensor clusters, International Journal of Sensor Networks 1 (1/2) (2006) 34–40.
[43] M. Cardei, J. Wu, M. Lu, Improving network lifetime using sensors with adjustable sensing ranges, International Journal of Sensor Networks 1 (1/2) (2006) 41–49.
[44] S. Misra, G. Xue, Efficient anonymity schemes for clustered wireless sensor networks, International Journal of Sensor Networks 1 (1/2) (2006) 50–63.
[45] H. Zhang, J.C. Hou, Maximising α-lifetime for wireless sensor networks, International Journal of Sensor Networks 1 (1/2) (2006) 64–71.
[46] R.W. Ha, P.-H. Ho, X. Shen, Optimal sleep scheduling with transmission range assignment in application-specific wireless sensor networks, International Journal of Sensor Networks 1 (1/2) (2006) 72–88.

[47] U. Korad, K.M. Sivalingam, Reliable data delivery in wireless sensor networks using distributed cluster monitoring, International Journal of Sensor Networks 1 (1/2) (2006) 75–83.
[48] S. Dulman, M. Rossi, P. Havinga, M. Zorzi, On the hop count statistics for randomly deployed wireless sensor networks, International Journal of Sensor Networks 1 (1/2) (2006) 89–102.
[49] G. Li, T. Znati, A. Gopalan, REAP: ring band-based energy adaptive protocol for information dissemination and forwarding in wireless sensor networks, International Journal of Sensor Networks 1 (1/2) (2006) 103–113.
[50] J. Misic, V. Misic, Editorial, International Journal of Sensor Networks 1(3/4) (2006) 115–116.
[51] Z. Liu, I. Elhanany, RL-MAC: a reinforcement learning based MAC protocol for wireless sensor networks, International Journal of Sensor Networks 1 (3/4) (2006) 117–124.
[52] C.K. Nguyen, A. Kumar, Energy-efficient medium access control with throughput optimisation for wireless sensor networks, International Journal of Sensor Networks 1 (3/4) (2006) 125–133.
[53] M. Ali, Z. Uzmi, Medium access control with mobility-adaptive mechanisms for wireless sensor networks, International Journal of Sensor Networks 1 (3/4) (2006) 134–142.
[54] M. Moh, E. Kim, T.-S. Moh, Design and analysis of distributed power scheduling for data aggregation in wireless sensor networks, International Journal of Sensor Networks 1 (3/4) (2006) 143–155.
[55] K. Sha, J. Du, W. Shi, WEAR: a balanced (fault-tolerant) energy-aware routing protocol in WSNs, International Journal of Sensor Networks 1 (3/4) (2006) 156–168.
[56] V. Vivekanandan, V.W.S. Wong, Ordinal MDS-based localisation for wireless sensor networks, International Journal of Sensor Networks 1 (3/4) (2006) 169–178.
[57] W. Chen, S.-Y. Kuo, H.-C. Chao, Fuzzy preserving virtual polar coordinate space sensor networks for mobility performance consideration, International Journal of Sensor Networks 1 (3/4) (2006) 179–189.
[58] S.-C. Huang, R.-H. Jan, W. Yang, RICA: a ring-based information collection architecture in wireless sensor networks, International Journal of Sensor Networks 1 (3/4) (2006) 190–199.
[59] I. Solis, K. Obraczka, In-network aggregation trade-offs for data collection in wireless sensor networks, International Journal of Sensor Networks 1 (3/4) (2006) 200–212.
[60] N. Tezcan, W. Wang, TTS: a two-tiered scheduling mechanism for energy conservation in wireless sensor networks, International Journal of Sensor Networks 1 (3/4) (2006) 213–228.
[61] S. Lin, V. Kalogeraki, D. Gunopulos, S. Lonardi, Efficient information compression in sensor networks, International Journal of Sensor Networks 1 (3/4) (2006) 229–240.
[62] R. Khanna, H. Liu, H.-H. Chen, Self-organisation of sensor networks using genetic algorithms, International Journal of Sensor Networks 1 (3/4) (2006) 241–252.
[63] X. Jia, H. Du, Editorial, International Journal of Sensor Networks 2 (1/2) (2006) 1–2.
[64] J. Chen, Y. Sun, Dynamic priority scheduling-based MAC for wireless sensor networks, International Journal of Sensor Networks 2 (1/2) (2006) 3–8.
[65] A. Mayank, C.V. Ravishankar, Supporting mobile device communications in the presence of broadcast servers, International Journal of Sensor Networks 2 (1/2) (2006) 9–16.
[66] L. Huang, H. Xu, Y. Wan, J. Wu, H. Li, An efficient synchronisation protocol for wireless sensor network, International Journal of Sensor Networks 2 (1/2) (2006) 17–24.
[67] G. Jin, S. Nittel, UDC: a self-adaptive uneven clustering protocol for dynamic sensor networks, International Journal of Sensor Networks 2 (1/2) (2006) 25–33.
[68] G. Li, T. Znati, RECA: a ring-structured energy-efficient clustering architecture for robust communication in wireless sensor networks, International Journal of Sensor Networks 2 (1/2) (2006) 34–43.
[69] H. Ma, Y. Liu, Some problems of directional sensor networks, International Journal of Sensor Networks 2 (1/2) (2006) 44–52.
[70] J. Li, J. Li, Data sampling control, compression and query in sensor networks, International Journal of Sensor Networks 2 (1/2) (2006) 53–61.
[71] S. Zhao, L. Tan, J. Li, A distributed energy efficient multicast routing algorithm for WANETs, International Journal of Sensor Networks 2 (1/2) (2006) 62–67.
[72] Z. Yuanyuan, J. Xiaohua, H. Yanxiang, A distributed algorithm for constructing energy-balanced connected dominating set in wireless sensor networks, International Journal of Sensor Networks 2 (1/2) (2006) 68–76.
[73] K. Kim, J. Jeon, K. Yoo, Efficient and secure password authentication schemes for low-power devices, International Journal of Sensor Networks 2 (1/2) (2006) 77–81.
[74] Y. Lee, J. Lee, V. Phadke, A. Deshmukh, Location verification using bidirectional one-way hash function in wireless sensor networks, International Journal of Sensor Networks 2 (1/2) (2006) 82–90.
[75] Y. Xiao, H. Chen, K. Wu, B. Sun, Y. Zhang, X. Sun, C. Liu, Coverage and detection of a randomized scheduling algorithm in wireless sensor networks, IEEE Transactions on Computers, under review.

Yang Xiao worked in industry as a MAC (Medium Access Control) architect involving the IEEE 802.11 standard enhancement work before he joined Department of Computer Science at The University of Memphis in 2002. He is currently with Department of Computer Science at The University of Alabama. He was a voting member of IEEE 802.11 Working Group from 2001 to 2004. He is an IEEE Senior Member. He is a member of American Telemedicine Association. He currently serves as Editor-in-Chief for *International Journal of Security and Networks* (IJSN), *International Journal of Sensor Networks* (IJSNet), and *International Journal of Telemedicine and Applications* (IJTA). He serves as a referee/reviewer for many funding agencies, as well as a panelist for NSF and a member of Canada Foundation for Innovation (CFI)'s Telecommunications expert committee. He serves on TPC for more than 100 conferences such as INFOCOM, ICDCS, MOBIHOC, ICC, GLOBECOM, and WCNC. He serves as an associate editor for several journals, e.g., *IEEE Transactions on Vehicular Technology*. His research areas are security, telemedicine, sensor networks, and wireless networks. He has published more than 300 papers in major journals, refereed conference proceedings, book chapters related to these research areas. His research has been supported by the US National Science Foundation (NSF), US Army Research, Fleet & Industrial Supply Center San Diego (FISCSD), and The University of Alabama's Research Grants Committee. Dr. Xiao is a Guest Professor of Jilin University, and an Adjunct Professor of Zhejiang University.

Yanping Zhang is currently pursuing the Ph.D. degree in Computer Science at The University of Alabama. She received the B.E. degree in Electrical Engineering from Zhengzhou University, Zhengzhou, China, in 1999. She was awarded the Excellent Graduation Student of He'nan province, China, in 1999. She currently is a research assistant at The University of Alabama. Her research interests include Medium Access Control (MAC) layer optimization in wireless sensor networks (WSNs), intrusion detection in WSNs, wireless network security, protection from cyber crime, bio-inspired application in sensor networks, and telemedicine.

Miao Peng received the B.S. degree in Applied Mathematics from Dalian University of Technology, Dalian, China, in 2004, and the M.S. degree in Mathematical Statistics from Jilin University, Changchun, China, in 2007. He is currently pursuing the Ph.D. degree in Computer Science at The University of Alabama. He currently is a research assistant at The University of Alabama. His research interests include wireless sensor network, wireless network security, energy efficient wireless network. In particular, he is interested in mathematical modeling in wireless and sensor networks.

Hui Chen is a geophysicist turned computer programmer and computer science researcher. From 1996 to 2001, he spent most of his time in research on computational aspects of geophysics. He late worked as a software developer in industry. Out of his interest in research and teaching, and his desire to learn, he joined the faculty of the Department of Mathematics and Computer Science at Virginia State University in 2007. While retaining interest in computational problems in Earth sciences, he primarily works on computer systems, networking, and security areas such as design and analysis wireless networks, sensor networks, caching for wireless systems, operating system and network security as well as applied computing. He served and is serving as technical program committee member for many conferences such as IEEE Globecom and IEEE ICC. He was and is a guest editor of a few journals, such as special issues of "Wireless Telemedicine and Applications" and "Wireless Network Security" of the EURASIP Journal on Wireless Communications and Networking. He is member of IEEE and ACM.

Dr. Xiaojiang (James) Du joins the Department of Computer and Information Sciences at Temple University in Fall 2009. Dr. Du was an Assistant Professor in the Department of Computer Science at North Dakota State University from August 2004 to July 2009. He received the Excellence in Research Award from the College of Science and Math at North Dakota State University in May 2009. Dr. Du earned his B.E. degree from Tsinghua University, Beijing, China in 1996, and his M.S. and Ph.D. degrees from the University of Maryland, College Park in 2002 and 2003, respectively, all in Electrical Engineering. His research interests are wireless networks, security, computer networks and systems. Dr. Du has authored over 70 peer-reviewed journal and conference papers in these areas. Dr. Du has been awarded more than $1M research grants from the US National Science Foundation, Army Research Office, and other sources. He is an Editor of four international journals: Wireless Communication and Mobile Computing (Wiley), Security and Communication Networks (Wiley), Journal of Computer Systems, Networking, and Communications (Hindawi), and International Journal of Sensor Networks (InderScience). Dr. Du is (was) the Chair of Computer and Network Security Symposium of the IEEE/ACM International Wireless Communication and Mobile Computing Conference in 2006, 2007, 2008 and 2009. He is (was) a Technical Program Committee member of several premier IEEE conferences such as INFOCOM (2007–2010), IM, NOMS, ICC, GLOBECOM, WCNC, BroadNet, and IPCCC.

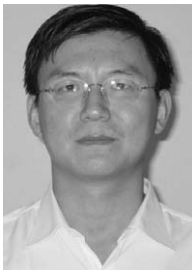

Bo Sun received his Ph.D. degree in Computer Science from Texas A&M University, College Station, USA, in 2004. He is now an assistant professor in the Department of Computer Science at Lamar University, USA. His research interests include the security issues (intrusion detection in particular) of Wireless Ad Hoc Networks, Wireless Sensor Networks, Cellular Mobile Networks, and other communications systems. His research has been supported by the Texas Higher Education Coordination Board's Advanced Research Program (ARP) and the US National Science Foundation (NSF).

Kui Wu received the Ph.D. degree in computing science from the University of Alberta, Canada in 2002. He then joined the Department of Computer Science, University of Victoria, Canada, where he is currently an Associate Professor. His research interests include mobile and wireless networks, sensor networks, network performance evaluation, and network security.